Exp Fluids (2011) 50:1443–1453
DOI 10.1007/s00348-010-1003-0

RESEARCH ARTICLE

Spatial resolution correction for hot-wire anemometry in wall turbulence

C. Chin · N. Hutchins · A. Ooi · I. Marusic

Received: 18 July 2010 / Revised: 29 September 2010 / Accepted: 21 October 2010 / Published online: 13 November 2010

Abstract We investigate spatial resolution issues in hot-wire anemometry measurements of turbulence intensity and energy spectra. Single normal hot-wire measurements are simulated by means of filtering direct numerical simulation (DNS) of turbulent channel flow at $Re_\tau = 934$. Through analysis of the two-dimensional energy spectra from the DNS, the attenuation of the small-scale energy levels is documented, especially in the near-wall region. The missing energy displays anisotropic characteristics, and an attempt is made to model this using an empirical equation, thus providing a correction scheme for all wall normal locations. The empirical model is assessed using experimental boundary layer data and shown to effectively correct both the streamwise one-dimensional energy spectra and turbulence intensity at a Reynolds number significantly above that of the DNS.

1 Introduction

Hot-wire anemometry (HWA) is widely utilized in turbulence research of wall-bounded flows, where its temporal and spatial resolution is largely unmatched by other experimental techniques. In spite of these obvious advantages, the ability of HWA to provide accurate measurements, especially in the near-wall region at high Reynolds numbers, remains an issue. This is due to the finite spatial resolution of the sensing element and its inability to capture the very small scales that occur in the near-wall as discussed by Johansson and Alfredsson (1983), Ligrani and Bradshaw (1987) and Hutchins et al. (2009). The pursuit to obtain accurate HWA measurements has lead many researchers to formulate corrections for turbulence statistics acquired by HWA. The earliest correction methods proposed by Dryden et al. (1937), Frenkiel (1949), Corrsin and Kovasznay (1949), Wyngaard (1968) and Roberts (1973) were largely theoretical and based on the assumption of isotropic turbulence. However, the assumption of isotropic turbulence is not applicable in wall-bounded flows, as turbulent structures are shown to be highly anisotropic as reported by Kline et al. (1967), Smith and Metzler (1983) and del Álamo and Jiménez (2003). With the availability of DNS data, spatial resolution effects in HWA can be simulated by means of spatially averaging the DNS data. Suzuki and Kasagi (1992) used DNS channel flow to investigate the spatial resolution effects for cross-wire probes and proposed a correction method using two-point correlation functions. Later, Buranttini et al. (2007) introduced corrections for single normal hot-wire for under-resolved scalar measurements using DNS of homogeneous isotropic turbulence. Recently, Chin et al. (2009) utilized DNS channel flow data at moderate Reynolds number and proposed an empirical correction limited to wall-normal location of $z^+ = 15$, where the symbol '+' denotes scaling with viscous length scale, ν/u_τ, where ν is the viscosity, and u_τ is the streamwise friction velocity. The streamwise, spanwise and wall-normal directions are defined as x, y and z, respectively.

In this paper, we investigate the spatial attenuation effects of HWA on different turbulence statistics, such as turbulence intensity and energy spectra. In addition, we look to extend the empirical missing energy model of Chin

C. Chin (✉) · N. Hutchins · A. Ooi · I. Marusic
Department of Mechanical Engineering,
University of Melbourne, Melbourne,
VIC, Australia
e-mail: chincc@unimelb.edu.au

N. Hutchins
e-mail: nhu@unimelb.edu.au

et al. (2009) to account for spatial attenuation for all wall-normal heights. To the authors knowledge, this is the first time that such a correction scheme is proposed to correct one-dimensional streamwise energy spectra for different hot-wire lengths across all wall-normal locations up to δ (which is the half channel height or boundary layer thickness). The empirical missing energy model will be applied to experimental data to verify its validity.

2 Numerical analysis

The DNS channel flow data used in this study is by del Álamo et al. (2004). The Reynolds number is $Re_\tau = u_\tau \delta / \nu \approx 934$, and the streamwise, spanwise and wall-normal fluctuating velocity components are u, v and w. The computational domain is $L_x \times L_y \times L_z = 8\pi\delta \times 3\pi\delta \times 2\pi\delta$, and the spatial resolutions in x and y are $\Delta x^+ \approx 7.6$ and $\Delta y^+ \approx 3.8$. Spacing (Δz^+) in the wall-normal direction is with Chebychev polynomials with spatial resolutions ranging between [0.03, 7.64]. Readers are referred to the paper by del Álamo et al. (2004) for more details of the DNS data. The signal attenuation due to finite hot-wire length is simulated by means of spatially averaging the streamwise velocity from the DNS along the spanwise direction. The methodology to filter and process the DNS data is the same as that employed by Chin et al. (2009). With the given fixed spanwise spatial resolution of $\Delta y^+ \approx 3.8$, the filter lengths are limited to multiplies of Δy^+. In this study, the filter lengths considered are $l^+ \approx 3.8$ (unfiltered), 11.5 $(3\Delta y^+)$, 19.1 $(5\Delta y^+)$, 34.4 $(9\Delta y^+)$, 57.3 $(15\Delta y^+)$, 80.2 $(21\Delta y^+)$ and 156.6 $(41\Delta y^+)$. After filtering the DNS data with the desired filter lengths, the one- and two-dimensional premultiplied energy spectra are calculated by

$$\psi_{uu}(k_x, z) = k_x \langle \hat{u}(k_x, z) \hat{u}^*(k_x, z) \rangle, \quad (1)$$

for one-dimensional premultiplied energy spectra and

$$\Psi_{uu}(k_x, k_y, z) = k_x k_y \langle \hat{u}(k_x, k_y, z) \hat{u}^*(k_x, k_y, z) \rangle, \quad (2)$$

for two-dimensional premultiplied energy spectra. The streamwise and spanwise wavenumbers are denoted by k_x and k_y (where $k = 2\pi/\lambda$, λ is the wavelength), the $\langle\ \rangle$ denotes temporal average, $\hat{u}$ denotes Fourier transform of u, and * denotes complex conjugate. The missing one and two-dimensional premultiplied energy spectra can then be easily calculated by subtracting the filtered energy spectra (computed based on the desired l^+) from the unfiltered energy spectra ($l^+ = 3.8$).

3 Insufficient spatial resolution effects

The effects of insufficient resolution can clearly be seen in the attenuation of the turbulence intensity $\overline{u^+}^2 = (\overline{u}/u_\tau)^2$ in

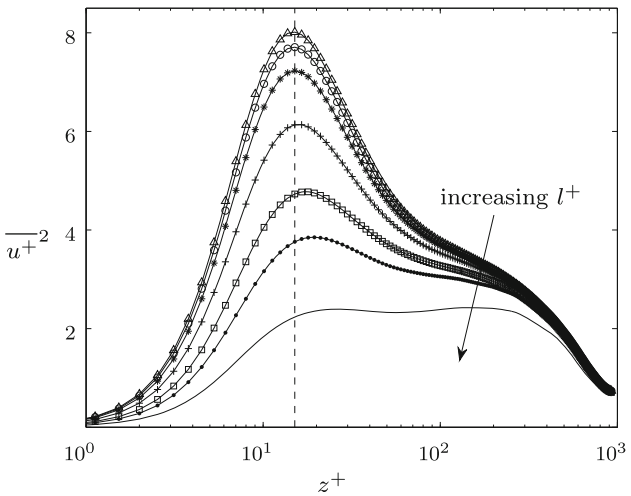

Fig. 1 Attenuated turbulence intensity profiles for different filter lengths applied on DNS data, $l^+ \approx 3.8$ (*triangle*), 11.5 (*circle*), 19.1 (*asterisk*), 34.3 (*plus*), 57.3 (*square*), 80.2 (*bullet*) and 156.6 (*solid line*), *arrow* indicates increasing filter length (l^+), the *dashed line* is at $z^+ \approx 15$

Fig. 1. Here, the different profiles symbolize different filter lengths (l^+) applied to the DNS data. It is clear that as the filter length increases, the amount of attenuation on the signal increases significantly. The effect of insufficient spatial resolution seems to be more prominent in the near-wall region, which is as expected, since this is where the majority of small-scale turbulent motions are situated. It is also interesting to note that the attenuation gradually decreases with increasing wall-normal distance and appears to diminish completely as z approaches the half channel height δ, for all but the longest simulated wire-length. The peak turbulence intensity at wall-normal location of $z^+ = 15$ (shown as dashed line in Fig. 1) suffers the greatest attenuation. The amount of attenuation at $z^+ = 15$ caused by different filter lengths when compared to the 'true turbulence intensity' is summarized in Table 1. It is widely accepted that the peak turbulence intensity occurs close to $z^+ \approx 15$ due to the near-wall cycle of quasi-streamwise vortices (see for example Kline et al. 1967;

Table 1 Tabulated attenuation of turbulence intensity in percentage (%) for different wire-lengths at $z^+ \approx 15$

Filter length (l^+)	Symbol	$\overline{u^+}^2$ (*attenuation*, %)
3.8 (unfiltered)	Δ	–
11.5	○	3.8
19.1	*	9.8
34.4	+	23.5
57.3	□	41.0
80.2	•	53.1
156.6	–	72.1

Jeong et al. 1997). Small-scales are primarily dominant in the near-wall and are most susceptible to the influence of finite wire-length. To better understand this attenuation, we will investigate next the filtered one-dimensional premultiplied energy spectra, which will give a clearer picture of precisely which energetic scales are attenuated by spatial filtering and where such scales are situated.

The one-dimensional premultiplied energy spectra of streamwise fluctuations are shown in Fig. 2. The spectra maps show the one-dimensional premultiplied energy spectra $\psi^+_{uu} = \psi_{uu}/u^2_\tau$ as a function of streamwise wavelength (λ^+_x) and wall-normal location (z^+). The contour maps are colored-scaled for $\psi^+_{uu} = 0.4$–2.0 (color-scale at bottom of plot). Such spectrograms are useful, since they readily show the energetic scales present at the wall-normal locations throughout the shear-layer. The figures have certain readily identifiable features. Primarily, there is a pronounced near-wall energetic peak located at $z^+ = 15, \lambda^+_x = 1{,}000$. This peak is documented in Hutchins and Marusic (2007) and is attributed to the near-wall cycle. This peak is clearly evident in the unfiltered results of Fig. 2a and is marked with a '+' symbol. Please note that throughout the text, the inner and outer energetic peaks refer to the peaks in the spectrogram of 1d premultiplied energy spectra as shown in Fig. 2 (and later Figs. 6, 7). In addition, Hutchins and Marusic (2007) note that at sufficient Reynolds number, turbulent boundary layers exhibit a secondary larger scale peak, located at $z^+/\delta^+ \approx 0.05, \lambda^+_x/\delta^+ \approx 6$ (this wall location was later refined by Mathis et al. (2009) to $z^+ \approx 3.9(Re_\tau)^{0.5}$). This peak has been attributed to the superstructures or the very large-scale motions (Kim and Adrian 1999) that populate the logarithmic region. For internal geometries, the location of this very large-scale energy differs slightly from that of turbulent boundary layers (see Monty et al. 2009; Hutchins et al. 2009). In this instance, the Reynolds number is quite low, and the large-scale energy is not yet fully developed, or sufficiently separated in scale from the near-wall motion, to adequately discern the large-scale peak (in these 1d spectra maps). However, Fig. 2a seems to indicate that this peak is located at approximately $z^+ = 0.15\delta^+, \lambda^+_x = 10\delta^+$. This location is marked on Fig. 2 using the 'X' symbol. The spatial attenuation of the small scales is clearly illustrated as the filter length increases from $l^+ = 19.1$ (Fig. 2b) to $l^+ = 156.6$ (Fig. 2d). Figure 2 shows

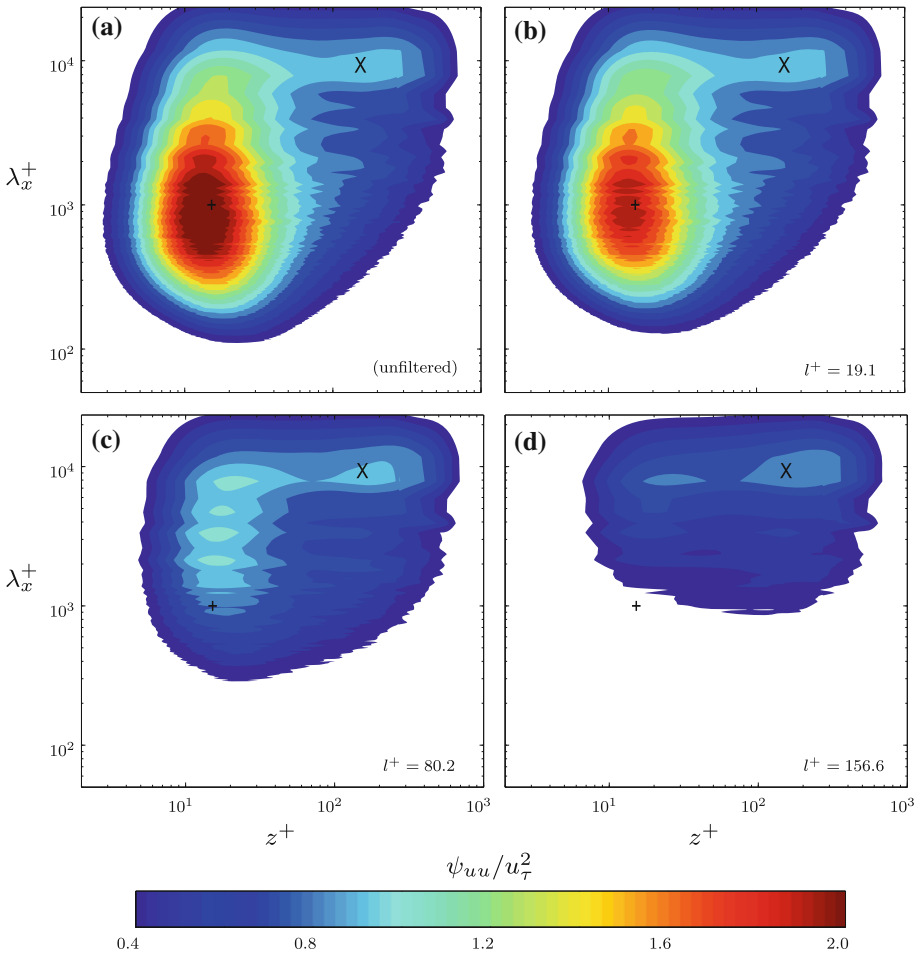

Fig. 2 Effect of spatial attenuation on the premultiplied one-dimensional streamwise energy spectra ψ_{uu}/u^2_τ from wall-normal locations $z^+ = 0$ to δ for different filter lengths **a** unfiltered, **b** $l^+ \approx 19.1$, **c** $l^+ \approx 80.2$ and **d** $l^+ \approx 156.6$ applied on the DNS data. The symbols '+' ($z^+ = 15, \lambda^+_x = 1{,}000$) and 'X' ($z^+ = 0.15\delta^+, \lambda^+_x = 10\delta^+$) denote inner and outer sites, respectively. Outer-most contour starts at 0.4 with increment of 0.35

evidence that the energy attenuation is largely confined to the near-wall, with the peak energy around the inner site severely attenuated as the filter length increases. The effect of insufficient spatial resolution is considerably less in the outer region, where the magnitude and population of small-scale energy is less. The attenuation of the small scales near the wall causes the peak energy to shift to a greater wavelength, which potentially could be misinterpreted as indicating large-scale dominance in the near-wall region. It is therefore imperative to account for the spatial attenuation caused by large hot-wires.

The effects of insufficient spatial resolution on the two-dimensional premultiplied energy spectra ($\Psi^+_{uu} = \Psi_{uu}/u^2_\tau$) are highlighted in Fig. 3. The 2d spectrograms show the spectra energy at corresponding streamwise wavelengths λ^+_x (x-axis) and spanwise wavelengths λ^+_y (y-axis) at wall-normal location $z^+ \approx 15$. Figure 3a–c show the 2d spectra for filter lengths of $l^+ \approx 3.8$ (unfiltered), 34.4 and 57.3, respectively. Contour maps begin at $\Psi^+_{uu} = 0.25$ with increments of 0.25. The '*' symbol indicates the peak of the unfiltered 2d spectra (see Fig. 3a) and is located at $\lambda^+_x \approx 700$ and $\lambda^+_y \approx 110$. This is similar to the wall region 2d spectra peak location of $\lambda^+_x \approx 700$ and $\lambda^+_y \approx 100$ as reported by del Álamo and J. Jiménez (2001). Here, the small-scale region is defined as the region enclosed by the dashed lines where wavelengths are of $\lambda^+_x < 2{,}000$ and $\lambda^+_y < 300$. The large-scale region is defined as having wavelengths of either $\lambda^+_x > 2{,}000$ and/or $\lambda^+_y > 300$. The plots in Fig. 3 clearly show that the attenuation of the 2d spectra is largely confined to the vicinity of the 2d spectra peak. The 2d spectra in the large-scale region seems to be unaffected by insufficient spatial resolution. The missing two-dimensional premultiplied energy spectra due to spatial attenuation are shown in Fig. 4. The contour maps show the missing energy at three different wall-normal locations of $z^+ = 5$, 15 and 32 using a constant filter length of $l^+ \approx 34.4$. The dark contours represent the attenuated energy due to filtering of the DNS data. The attenuated energy is calculated by subtracting the filtered 2d energy spectra from the unfiltered 2d energy spectra. For example, the missing energy in Fig. 4b is obtained by subtracting the filtered 2d energy spectra of Fig. 3b from the unfiltered 2d energy spectra of Fig. 3a. The gray contours show an attempt to model the missing energy using the functional form described in Eq. 3 and developed in Sect. 4

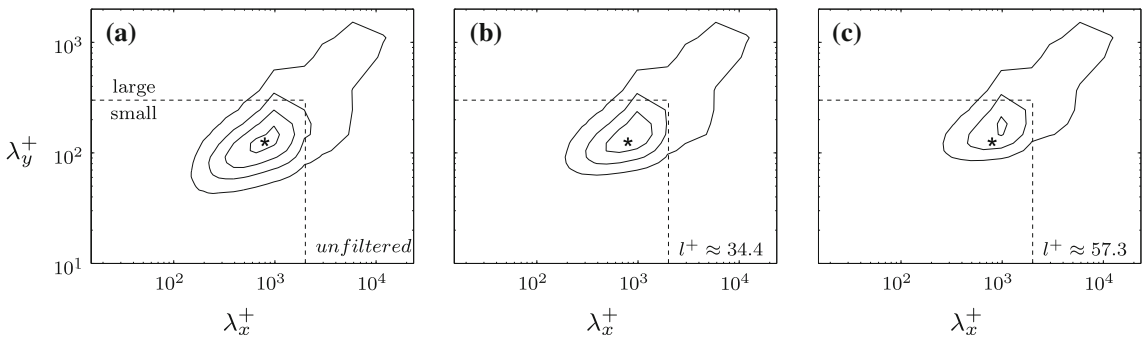

Fig. 3 Premultiplied streamwise two-dimensional missing energy spectra $\Psi^+_{uu} = \Psi_{uu}/u^2_\tau$ at wall-normal location $z^+ \approx 15$ for different filter lengths; **a** $l^+ \approx 3.8$ (unfiltered), **b** $l^+ \approx 34.4$ and **c** $l^+ \approx 57.3$. Contour maps begin at 0.25 with increment of 0.25. The '*' symbol is at location $\lambda^+_x \approx 700$ and $\lambda^+_y \approx 110$. The *dashed lines* encloses the region $\lambda^+_x < 2{,}000$ and $\lambda^+_y < 300$

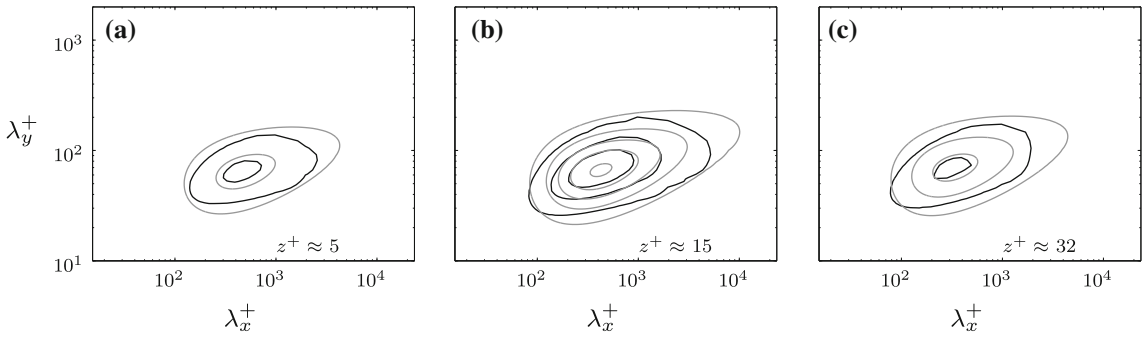

Fig. 4 Premultiplied streamwise two-dimensional missing energy spectra $\Psi^+_{uu} = \Psi_{uu}/u^2_\tau$ at wall-normal location; **a** $z^+ \approx 5$, **b** $z^+ \approx 15$, **c** $z^+ \approx 32$ for filter length of $l^+ \approx 34.4$. Contour maps begin at 0.05 with increment of 0.1. *Black contour lines* represent attenuated energy due to filtering, *gray contour lines* represent the missing energy model, given in Eq. 3

of this paper. The contour levels start at $\Psi^+_{uu} = 0.05$ with increment of 0.1. It is worth noting that the amount of attenuated energy increases as z^+ increases and is most severe at $z^+ = 15$ before decreasing as we move away from the wall. Figure 4 clearly shows that the attenuated energy is greater in the streamwise length scale (λ^+_x) than spanwise length scale (λ^+_x). This gives evidence that the attenuated energy is highly anisotropic and renders incorrect the assumption of homogeneous isotropic turbulence used in some previous correction schemes.

4 Model for missing energy spectra

By plotting the 2d spectra for the filtered DNS data, we can get a clearer understanding of the effects of limited spatial resolution. The 2d spectra plots of Figs. 3 and 4, and those shown previously by Chin et al. (2009), clearly demonstrate that spatial attenuation is restricted to wavelengths of $\lambda^+_x \sim O(1{,}000)$ and $\lambda^+_y \sim O(100)$. The large-scale energy (within the large-scale region shown in Fig. 3) is found to be relatively uneffected by spatial filtering as discussed previously. Such observations pave the way for the attempted correction scheme. Not only is the missing energy rather simple to model (as discussed below), but this confinement of attenuation to viscous-scales only suggests that a correction scheme could be formulated that, in theory, could work at much higher Reynolds numbers, and different flow geometries. Hutchins and Marusic (2007) have clearly demonstrated for boundary layer flows that as Reynolds number increases, it is only the large-scale energy that changes. The smaller viscous-scale energy remains the same. This implies that a correction scheme that can predict missing small-scale energy for a wire of a given length at low Reynolds number, ought, in theory, to be applicable for the same wire-length at much higher Reynolds number. In addition, comparisons of pipe, channel and flat plate boundary layers (see Monty et al. 2009) seem to indicate that the near-wall viscous scaled energy is the same in all three geometries, with only the largest scales exhibiting geometry dependence. This would seem to suggest that a correction scheme formulated using DNS data from channel flow ought to be applicable to pipe and turbulent boundary layer data.

The 2d spectra such as those shown in Fig. 4 enable one to model the missing energy in two-dimensional wavelength space as a function of various parameters such as wavelength (λ^+_x and λ^+_y), filter length (l^+) and wall-normal location (z^+). From Fig. 4, the missing energy seems to represent a symmetrical Gaussian in the λ^+_y axis and a skewed Gaussian in the λ^+_x axis that is slightly rotated counter-clockwise. Therefore, a proposed empirical expression is derived in the form

$$f(\lambda^+_x, \lambda^+_y, z^+, l^+) = A \exp\left(-\left[\frac{(\alpha-\alpha_0)^2}{\sigma_\alpha} + \frac{(\beta-\beta_0)^2}{\sigma_\beta}\right]\right), \tag{3}$$

based on curve-fitting to the filtered DNS data. As can be seen, f is essentially a 2d Gaussian, where α and β are defined such that the Gaussian is skewed in the λ^+_x, λ^+_y plane. The magnitude of the Gaussian (A) is a function of wire-length l^+ and wall-normal distance z^+. The centers of the Gaussian α_0 and β_0 are functions of l^+. The width of the Gaussian in λ^+_x is a function of z^+. The following expressions for the constants are obtained:

$$A = 0.55 \exp\left(\frac{-(z^+ - 13.5)^2}{(z^+ + 8)^{1.77}}\right) \times \left[3.1(0.9375 - \exp(-0.017 l^+))^{1.35} + 0.15 \exp\left(\frac{-(l^+ - 57)^2}{200}\right)\right] \tag{4}$$

$$\alpha = 0.9611 \log_{10}(\lambda^+_x) + 0.2764 \log_{10}(\lambda^+_y) + C1 \tag{5}$$

$$\beta = -0.2764 \log_{10}(\lambda^+_x) + 0.9611 \log_{10}(\lambda^+_y) + C2 \tag{6}$$

$$\alpha_0 = \log_{10}(3.6 l^+ + 280) \tag{7}$$

$$\beta_0 = \log_{10}(0.3 l^+ + 58) \tag{8}$$

$$\sigma_\alpha = \log_{10}(\lambda^+_x)^{1/C3}/14.5 \tag{9}$$

$$\sigma_\beta = 0.09 \tag{10}$$

$$C1 = \exp\left(\frac{-(z^+ + 22)^{3.2}}{(3.35 z^+)^{3.25}}\right)^{6/4.2} - 0.46 \tag{11}$$

$$C2 = \frac{1}{60}\exp\left(\frac{-z^{+2}}{10^2}\right) + \frac{1}{40}\exp\left(\frac{-z^{+2}}{2\times 10^3}\right) + \frac{1}{5}\exp\left(\frac{-z^{+2}}{3\times 10^3}\right) + 0.6 \tag{12}$$

$$C3 = 0.01 \exp\left(\frac{-(z^+ - 400)^2}{z^{+3.9}}\right) + 0.54. \tag{13}$$

It should be noted that Eq. 3 is formulated for filter lengths up to $l^+ \approx 60$. This is the longest filter length used in the filtering scheme to obtain the missing two-dimensional energy spectra. However, Eq. 3, in theory, can be applied to model missing energy attenuated by larger wire-lengths. (This will be shown later.), One should note that the primary purpose of Eq. 3 is to aid experimentalists to obtain a better approximation of the 'true' energy content where spatial resolution becomes a serious issue (i.e high Reynolds number experiments or close to the wall). It is not intended to promote the use of large wire-lengths. In order to validate the missing spectra

energy model (hereinafter referred to MSEM), Eq. 3 is first used to calculate the missing two-dimensional energy for the wire-length $l^+ = 34.4$ and wall-normal locations of $z^+ = 5, 15$ and 32 (as shown in Fig. 4). The results are plotted in gray contours in Fig. 4 and prove to be a reasonable approximation of the missing energy (dark contours) calculated by filtering the DNS data. From the two-dimensional missing energy spectra (using Eq. 3), one could essentially integrate across the spanwise wavelengths (λ_y^+) to obtain the one-dimensional missing premultiplied streamwise energy spectra using the equation

$$\phi^+_{uu\,\mathrm{missing}}(\lambda_x^+, z^+, l^+) = \int f(\lambda_x^+, \lambda_y^+, z^+, l^+) d\log(\lambda_y^+). \tag{14}$$

Having obtained the one-dimensional missing energy, one can easily add it to the experimental one-dimensional energy spectra results to obtain an approximation of the 'true' value. ('True' value here refers to the unfiltered DNS results with a spanwise grid spacing $\Delta_y^+ \approx 3.8$). In theory, one could also correct the one-dimensional energy spectra to match any desired wire-length. Equation 3 corrects to a simulated $l^+ \approx 3.8$. However, if one had experimental data at $l^+ \approx 60$, but wished instead to correct the energy to that which would be measured with $l^+ \approx 20$, it is a relatively simple procedure. The missing energy for Eq. 3 would merely be calculated for both wire-lengths, the difference of this predicted missing energy, when added to the original ($l^+ \approx 60$) data, would provide a prediction of the energy that would be measured with a wire of length $l^+ \approx 20$.

To demonstrate the usefulness of the proposed correction scheme, we next apply the correction scheme to the under-resolved data of Hutchins et al. (2009). These data were acquired at much higher Reynolds numbers ($Re_\tau \approx$ 7,400 and 14,000; 8 and 15 times greater than the DNS) and are particularly useful for this test, since multiple repeated measurements were made at fixed Reynolds number but with varying l^+ (all experimental data used here has l/d ratio greater than 200). Thus, not only do we have access to data that is deliberately spatially under-resolved, but we also have data with much better spatial resolution against which we can compare our corrected results. We have chosen two different wall-normal locations $z^+ \approx 15$ and 55 at $Re_\tau \approx 7{,}400$ to illustrate how MSEM can be applied to correct the attenuated experimental energy spectra. This is shown in Fig. 5. Figure 5a and b show the raw experimental data ($l^+ \approx 11$, 22 and 79) for wall-normal locations $z^+ \approx 15$ and 55, respectively. These two plots together clearly show that the attenuation of the small scales increases as the hot-wire length increases and that the amount of attenuation for a given wire-length l^+ decreases with wall-normal distance. Here, the energy spectra are corrected to the shortest wire-length of $l^+ \approx 11$, corresponding to the best spatial resolution for that set of experiments. The predicted missing energy from Eq. 14 corresponding to the experimental data of $l^+ \approx 22$ and 79 is plotted in Fig. 5c and d. By summing the predicted missing energy to the experimental data (Fig. 5a, b), the corresponding corrected energy spectra are calculated. These are shown in Fig. 5e and f, where excellent agreement is seen for the corrected spectra. Figure 6 shows the one-dimensional energy spectrogram ϕ^+_{uu} for $Re_\tau \approx 7{,}400$. The contour levels are the same as those used in Fig. 2. The inner site ('+') is located at $z^+ = 15$ and $\lambda_x^+ = 1{,}000$ and outer site 'X' is at $z^+ = 3.9(Re_\tau)^{0.5}$ and $\lambda_x^+ = 6\delta^+$. The actual experimental energy spectra for $l^+ \approx 11$, 22 and 79 are shown in Fig. 6a, b and d. It is expected that as the wire-length increases, the energy attenuation will become more severe (as discussed for DNS data). This is clearly shown in Fig. 6a, b and d with the near-wall peak becoming increasingly eroded as l^+ increases, whilst the outer energetic peak appears completely unaltered. Here, we will again be correcting the energy spectra to the shortest wire-length of $l^+ \approx 11$ as demonstrated in Fig. 5. By summing the predicted missing energy to the experimental data at $l^+ \approx 22$ and 79 (Fig. 6b, d), the corresponding corrected energy spectra are shown in Fig. 6c and e. The corrected energy spectra of Fig. 6c and e exhibit a close approximation to the most spatially resolved measurements ($l^+ \approx 11$) of Fig. 6a. A similar analysis is performed on the experimental boundary layer data at $Re_\tau \approx 14{,}000$ and is shown in Fig. 7. One should note that the longest wire-length in this experiment was $l^+ \approx 153$, while the missing energy model was only formulated up to filter lengths of $l^+ \approx 60$. However, the findings for $Re_\tau \approx 14{,}000$ are very much similar to those of $Re_\tau \approx 7{,}400$, with the correction scheme successfully restoring the attenuated spectra maps back to a form that is very close to the most resolved measurement. It should be noted that there is a slight over-correction in the vicinity of the near-wall peak as seen in Fig. 7c and e. In general, results for Figs. 6 and 7 clearly support the validity of the MSEM to correct energy spectra suffering from spatial attenuation both at higher Reynolds numbers and different geometries.

With the validation of MSEM on the correction of one-dimensional energy spectra, it is therefore promising to extend the use of MSEM to correct experimental streamwise turbulence intensity (since the attenuated turbulence intensity is essentially the integrand of the missing one-dimensional energy spectra shown in Eq. 14 or the direct double integrand of the missing two-dimensional energy spectra given in Eq. 3). Here, we will again use the same experimental boundary layer data of Hutchins et al. (2009)

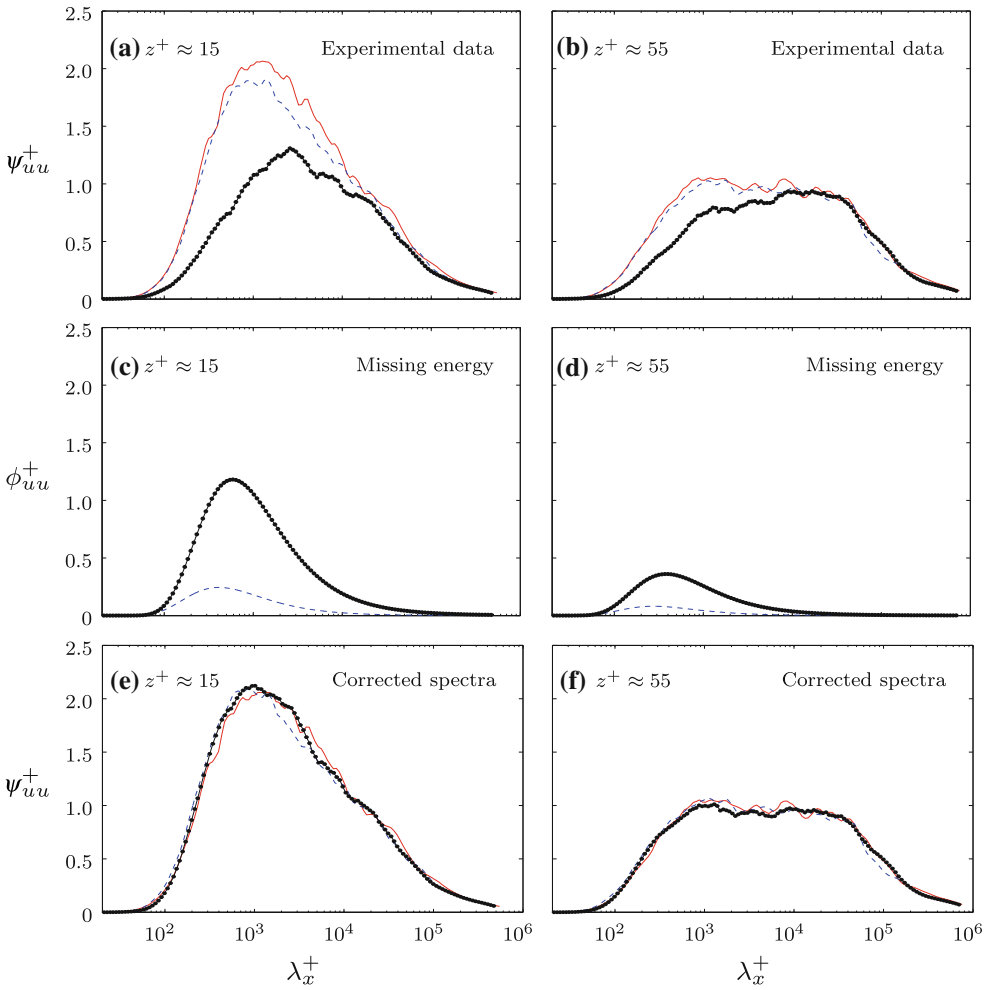

Fig. 5 Correction of one-dimensional energy spectra for $Re_\tau \approx 7{,}400$ at wall normal locations $z^+ \approx 15$ and 55. **a**, **b** Actual experimental results, **c**, **d** missing energy from Eq. 14, and **e**, **f** the corrected energy spectra to $l^+ \approx 11$. The symbols are of hot-wire lengths $l^+ \approx 11$ (*solid line*), $l^+ \approx 22$ (*dashed line*) and $l^+ \approx 79$ (*dot-dashed line*)

to validate the model for turbulence intensity corrections. Figure 8a and b show the experimental streamwise turbulence intensities for $Re_\tau \approx 7{,}400$ and 14,000, respectively. The effect of insufficient spatial resolution, resulting in the attenuation of the turbulence intensity in the near-wall region can clearly be seen. The attenuation, however, does not seem to effect the turbulence intensity towards the edge of the boundary layer. This is as expected, as previously discussed. The turbulence intensity profiles will be corrected to the shortest wire-length ($l^+ \approx 11$ for $Re_\tau \approx 7{,}400$ and $l^+ \approx 22$ for $Re_\tau \approx 14{,}000$). This is done by taking the integrand of the missing energy (either Eqs. 3 or 14) of the shortest wire-length and subtracting it from the integrand of the missing energy of the desired wire-length to be corrected. This is performed for all wall-normal locations where the turbulence intensity is to be corrected. Then, by adding the difference of the integrated missing energy, we will obtain the turbulence intensity profile corrected to the shortest wire-length. The corrected turbulence intensity profiles for $Re_\tau \approx 7{,}400$ and 14,000 are shown in Fig. 8c and d, respectively. The corrected results seem to agree well with actual measured data for the shortest hot-wire length. The MSEM appears to work remarkably well to correct high Reynolds numbers experimental results even though it is based on DNS data of $Re_\tau \approx 934$. These findings suggest that MSEM can be applied to correct actual experimental results despite the large difference in Reynolds number and external geometry.

5 Conclusion

We investigated the effects of insufficient spatial resolution on turbulence statistics by means of filtering DNS channel flow data to mimic finite hot-wire length. The turbulence intensity profiles show that the attenuation of turbulence intensity increases with filter length, especially at the near-wall peak. It is in the near-wall region where the most severe attenuation occurs due to the small scales (which are most susceptible to filtering) being more dominant in that region. In the outer region, spatial attenuation effect is less severe and seems to diminish towards the half channel

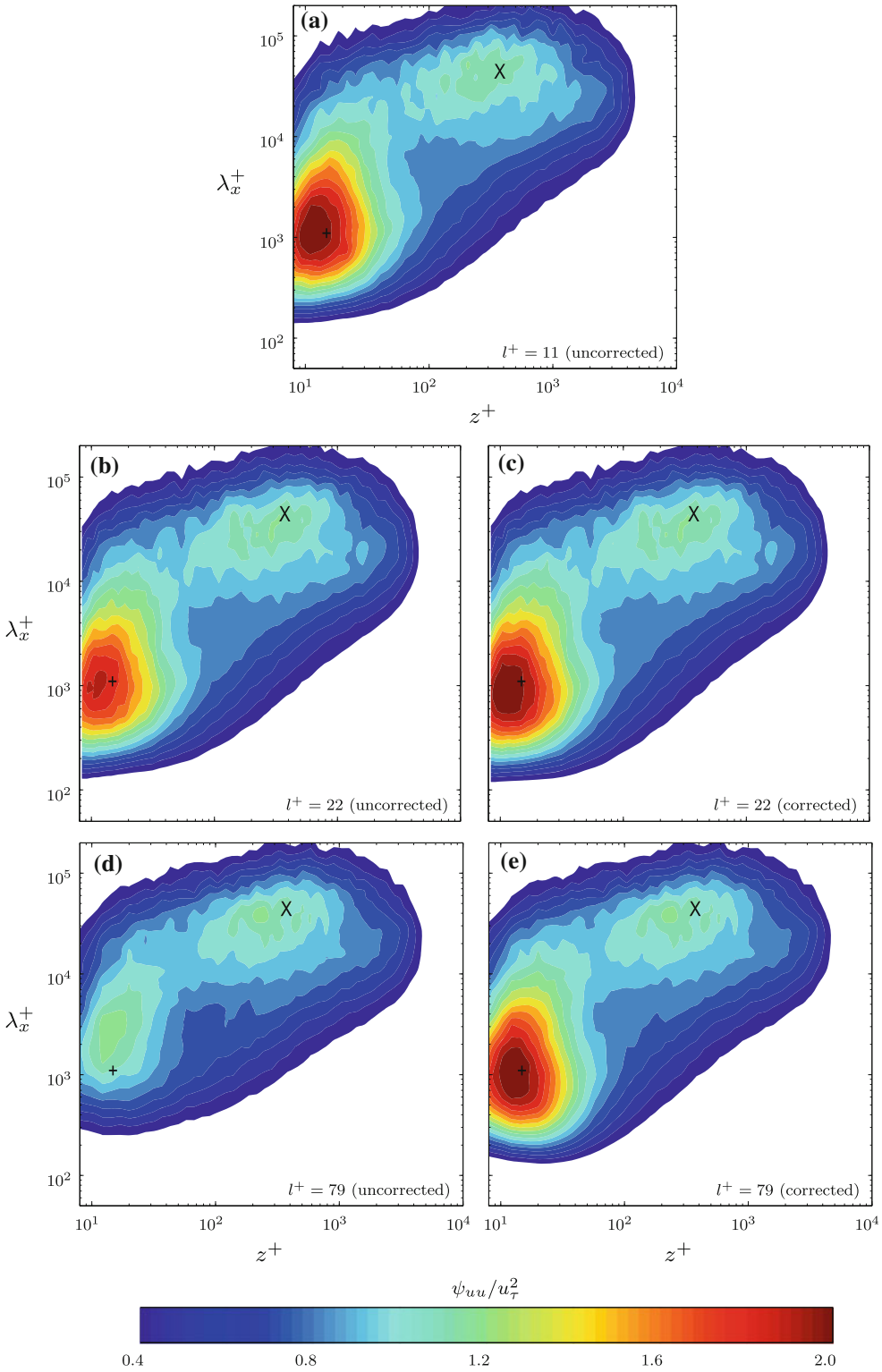

Fig. 6 Correction of boundary layer data using missing energy model (Eq. 3) at $Re_\tau \approx 7{,}400$ for hot-wire lengths $l^+ \approx 22$ and 79 to $l^+ \approx 11$. Inner site '+' ($z^+ = 15, \lambda_x^+ = 1{,}000$) and outer site 'X' ($z^+ = 3.9(Re_\tau)^{0.5}, \lambda_x^+ = 6\delta^+$). Actual experimental results **a** $l^+ \approx 11$, **b** $l^+ \approx 22$ and **d** $l^+ \approx 79$. Corrected experimental energy spectra **c** $l^+ \approx 22$ and **e** $l^+ \approx 79$ to $l^+ \approx 11$

height. The attenuation of the small scales in the near-wall is confirmed by the analysis of the one- and two-dimensional filtered premultiplied energy spectra. Using the two-dimensional missing energy from the filtered DNS data, we formulated an empirical model MSEM (Eq. 3) to model the missing energy. The MSEM can be used to model the missing two-dimensional energy spectra for all wall-normal locations up to δ and for filter length ranging from $3.8 < l^+ < 60$. With the use of MSEM, one will be able to account for the missing energy due to HWA attenuation

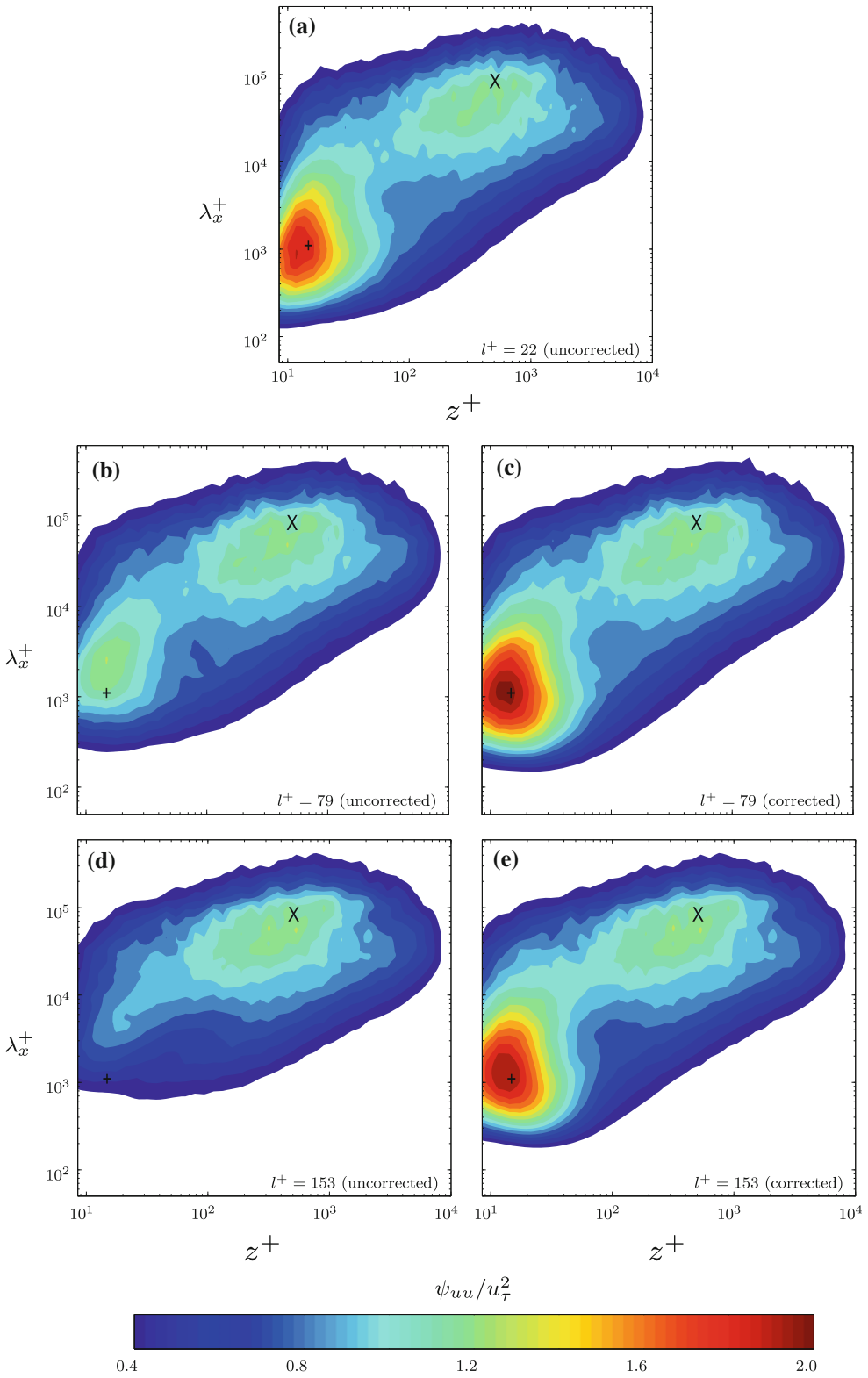

Fig. 7 Correction of boundary layer data using missing energy model (Eq. 3) at $Re_\tau \approx 14{,}000$ for hot-wire lengths $l^+ \approx 79$ and 153 to $l^+ \approx 22$. Actual experimental results **a** $l^+ \approx 22$, **b** $l^+ \approx 79$ and **d** $l^+ \approx 153$. Corrected energy spectra **c** $l^+ \approx 79$ and **e** $l^+ \approx 153$ to wire-length $l^+ \approx 22$. Symbols ('+', 'X') are as Fig. 6

effects. The real strength of this model is that it corrects the 2d energy spectra. Thus, not only is the correction more targeted (in terms of scales) but also allows one to recover corrected one-dimensional and two-dimensional spectra, rather than just mean intensities. A first integrand of the MSEM across the spanwise length scales will give us the missing one-dimensional energy spectra for a given wire-length. This missing streamwise one-dimensional energy

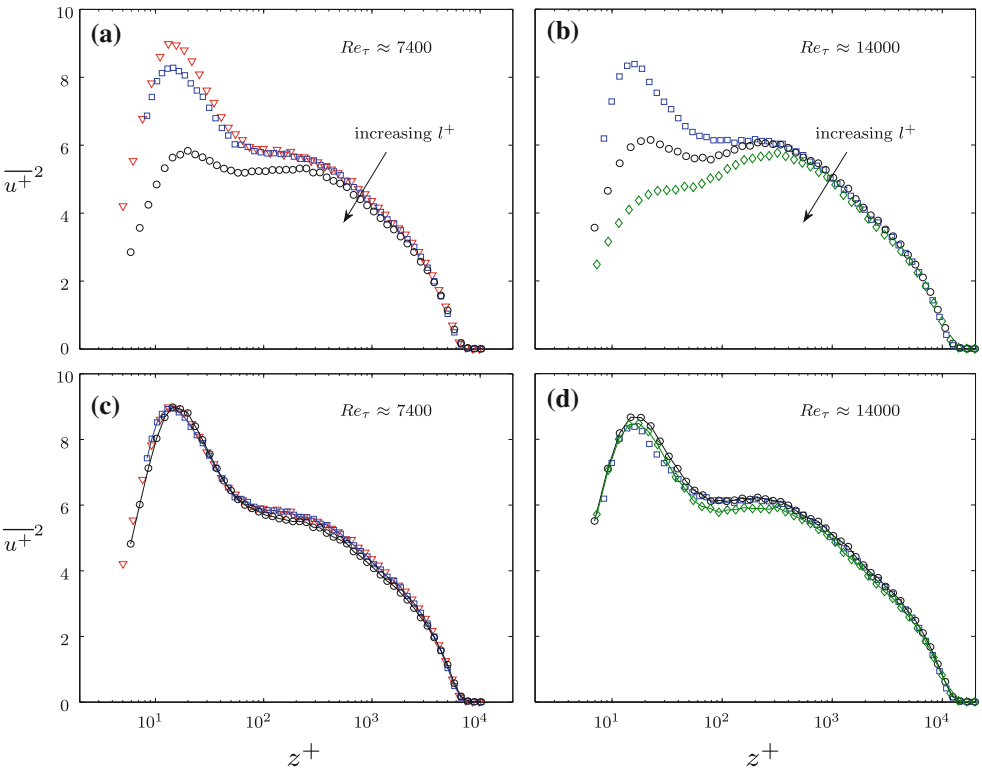

Fig. 8 Comparison of turbulence intensity profiles. Actual experimental results for filter lengths $l^+ \approx 11$ (*invertedtriangle*), $l^+ \approx 22$ (*square*), $l^+ \approx 79$ (*circle*), $l^+ \approx 153$ (*diamond*) for **a** $Re_\tau \approx 7{,}400$ and **b** $Re_\tau \approx 14{,}000$. **c** The corrected turbulence intensity to $l^+ \approx 11$ for $l^+ \approx 22$ (*square*), $l^+ \approx 79$ (*circle*) for $Re_\tau \approx 7{,}400$. And **d** the corrected turbulence intensity to $l^+ \approx 22$ for $l^+ \approx 79$ (*circle*), $l^+ \approx 153$ (*diamond*) for $Re_\tau \approx 14{,}000$

spectra can then be added to the experimental result to obtain the approximate 'true' value. A second integrand will present us with the missing turbulence intensity, which can be utilized to correct the turbulence intensity profiles of experimental results. The validation of MSEM is carried out using high Reynolds number boundary layer data of $Re_\tau \approx 7{,}400$ and 14,000 with largest wire-length of $l^+ \approx 153$ (Hutchins et al. 2009). The results obtained after correcting the data using MSEM ascertain the validity of the model. It seems that the vast difference in Reynolds number and larger wire-lengths has little effect on the overall feasibility of the model even though the MSEM does not account for Reynolds number effects or for wire-lengths greater than $l^+ \approx 60$. This is not really surprising. Attenuation due to insufficient spatial resolution is largely restricted to the viscous-scales. It is shown that these scales are uneffected by Reynolds number or geometry (Hutchins et al. 2009; Monty et al. 2009). Thus, it seems reasonable to suppose that a correction scheme formulated in a low Reynolds number channel flow should be applicable to a pipe or turbulent boundary layer at much higher Reynolds number. In other words, the only thing that changes as Reynolds number increases is the large-scale energy. Similarly, the only difference between internal and external geometries is in the large-scale energy. Since this portion of the signal will be uneffected by all but the most severe cases of spatial resolution, we might reasonably assume the measured (attenuated) signal to contain all relevant geometry and Reynolds number information. Hence, a simple additive correction scheme, such as the one proposed here, that merely replaces the missing 'universal' viscous-scales energy would seem to be a sensible approach. It is uncertain to what upper limit of Reynolds numbers or wire-length the MSEM will be valid. Presently, the MSEM seems sufficient to correct experimental results suffering from spatial attenuation up to $Re_\tau \approx 14{,}000$ and $l^+ \approx 153$.

Acknowledgments The authors wish to gratefully thank Prof. R. D. Moser for making the $Re_\tau = 934$, DNS data available, and the financial support of the Australian Research Council. The authors are also grateful for the support from Australian Partnership for Advanced Computing (APAC) and also Victorian Partnership for Advanced Computing (VPAC) for the computational time.

References

Burattini P, Kinet M, Carati D, Knaepen B (2007) Corrections for underresolved scalar measurements in turbulent flows using a dns database. Exp Fluids 43:31–37

Chin C, Hutchins N, Ooi A, Marusic I (2009) Use of direct numerical simulation (DNS) data to investigate spatial resolution issues in measurements of wall-bounded turbulence. Meas Sci Technol 20:115401

Corrsin S, Kovasznay LSG (1949) On the hot-wire length correction. Phys Rev 75:1954

del Álamo JC, Jiménez J (2001) Direct numerical simulation of the very large anisotropic scales in a turbulent channel. CTR Annual Research Briefs 2001, 329–341

del Álamo JC, Jiménez J (2003) Spectra of the very large anisotropic scales in turbulent channels. Phys Fluids 15:L41–L44

del Álamo JC, Jiménez J, Zandonade P, Moser RD (2004) Scaling of the energy spectra of turbulent channels. J Fluid Mech 500:135–144

Dryden HL, Shubauer GB, Moch WC, Skramstad HK (1937) Measurements of intensity and scale of wind tunnel turbulence and their relation of the critical reynolds number of spheres. NACA Technical Report 58

Frenkiel FN (1949) The influence of the length of a hot wire on the measurements of turbulence. Phys Rev 75:1263–1264

Hutchins N, Marusic I (2007) Evidence of very long meandering features in the logarithmic region of turbulent boundary layers. J Fluid Mech 579:1–28

Hutchins N, Nickels TB, Marusic I, Chong MS (2009) Hot-wire spatial resolution issues in wall-bounded turbulence. J Fluid Mech 635:103–136

Jeong J, Hussain F, Schoppa W, Kim J (1997) Coherent structures near the wall in a turbulent channel flow. J Fluid Mech 332:185–214

Johansson AV, Alfredsson PH (1983) Effects of imperfect spatial resolution on measurements of wall-bounded turbulent shear flows. J Fluid Mech 137:409–421

Kim KC, Adrian RJ (1999) Very large-scale motion in the outer layer. Phys Fluids 11(2):417–422

Kline SJ, Reynolds WC, Schraub FA, Runstandler PW (1967) The structure of turbulent boundary layer. J Fluid Mech 30:741–773

Ligrani PM, Bradshaw P (1987) Spatial resolution and measurement of turbulence in the viscous sublayer using subminiature hot-wire probes. Exp Fluids 5:407–417

Mathis R, Hutchins N, Marusic I (2009) Large-scale amplitude modulation of the small-scale structures of turbulent boundary layers. J Fluid Mech 628:311–337

Monty JP, Stewart JA, Williams RC, Chong MS (2007) Large-scale features in turbulent pipe and channel flows. J Fluid Mech 589:147–156

Monty JP, Hutchins N, Ng HCH, Marusic I, Chong MS (2009) A comparison of turbulent pipe, channel and boundary layer flows. J Fluid Mech 632:431–442

Roberts JB (1973) On the correction of hot wire turbulence measurements for spatial resolution errors. Aeronaut J 77:406–412

Smith CR, Metzler SP (1983) The characteristics of low-speed streaks in the near-wall region of a turbulent boundary layer. J Fluid Mech 129:27–54

Suzuki Y, Kasagi N (1992) Evaluation of hot-wire measurements in wall shear turbulence using a direct numerical simulation database. Exp Therm Fluid Sci 5:69–77

Wyngaard JC (1968) Measurement of small-scale turbulence structure with hot wires. J Phys E 1:1105–1108